Nanoscale

Accepted Manuscript

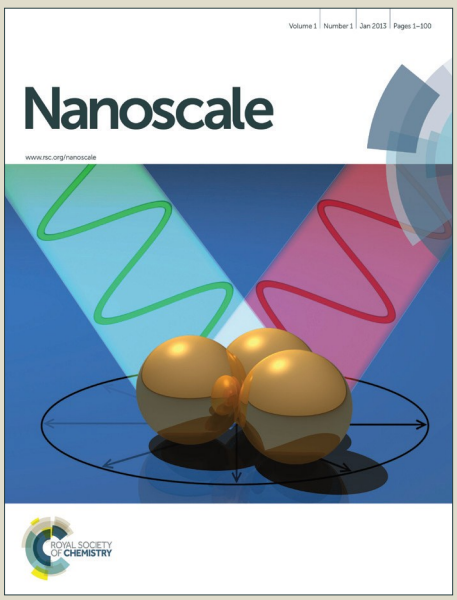

ROYAL SOCIETY OF CHEMISTRY

www.rsc.org/nanoscale

Journal Name

RSCPublishing

ARTICLE

Broadband Optical Limiting Response of Graphene-PbS Nanohybrid

Cite this: DOI: 10.1039/x0xx00000x

Min Zhao[a], Rui Peng[a], Qi Zheng[a], Qiang Wang[a]*, Meng-Jie Chang[a], Yu Liu[a], Ying-Lin Song[b,c]* and Hao-Li Zhang[a]*

Received 00th January 2012,
Accepted 00th January 2012

DOI: 10.1039/x0xx00000x

www.rsc.org/

Graphene-based materials have shown promising nonlinear optical properties in visible range. To extend their nonlinear optical response to the near infrared (NIR) region, we prepared a new nanohybrid consisting of uniform PbS quantum dots (QDs) attached on the reduced graphene oxide, named rGO-PbS, via a facile, low-cost, and phosphine-free method. The rGO-PbS nanohybrid exhibited superior optical limiting properties to either graphene oxide or PbS QDs upon both 532 nm and 1064 nm excitation in the nanosecond laser pulse regime, which is attributed to the synergetic effects stemming from charge transfer between the two components. Meanwhile, the thin films containing the rGO–PbS nanohybrid dispersed in polymethylmethacrylate (PMMA) also showed excellent optical limiting properties with high transparency, implying the potential applications of this hybrid material in broadband nonlinear optical devices.

Introduction

Nonlinear optical (NLO) materials are important for a variety of important technological applications including optoelectronic devices for telecommunications, information storage, optical switching, and signal processing[1-5]. Among various NLO materials, optical limiters, which exhibit high transmittance for low intensity laser pulses and low transmittance for high intensity input laser pulses, are particularly important for the applications like laser damage prevention and laser beam shaping[1-3, 6-9]. Significant progress has been made over recent decades in the development of various kinds of optical limiters, such as quantum dots (QDs)[10, 11], conducting polymer[12], organometallic compounds[4], small organic molecules[7] and inorganic carbon-based materials[13, 14].

NLO properties of graphene-based materials have attracted much attention lately[2, 3, 15]. It is found that few-layer graphene and graphene oxides (GO) exhibit induced saturable absorption transparency[2, 16, 17]. In solution, the saturable absorption behavior could switch to optical limiting at very high fluencies due to the nonlinear scattering from light-induced microbubbles and microplasma[3]. There are also several works reporting that GO optical limiting behavior is not only due to nonlinear scattering, but also to important two photon absorption (TPA) and/or excited state absorption[18-20]. However, because of the low band gap and high transparency nature, pristine graphene generally exhibits weak optical absorption, which is not ideal for optical limiting applications[21]. Recent researches have shown that attaching certain organic molecules or nanoparticles onto graphene can tune its absorption to obtain improved optical limiting performance[2, 8, 22, 23]. But only a few graphene-based materials exhibit high optical limiting properties at near-infrared (NIR) wavelength[24, 25], which can be attributed to their very low absorption in this region[22].

Seeking high performance optical limiters in the NIR region is important for many applications like telecommunication, sensing and certain military applications[9, 26-28]. Among various NIR active materials, lead chalcogenide colloidal QDs, particularly lead selenide (PbSe) QDs and lead sulfide (PbS) QDs, are the most widely studied ones, as they have low energy bandgap and high absorption coefficient in NIR region[29]. Previous studies on the third order nonlinear performance of several lead chalcogenide QDs[10, 28, 30, 31] have observed either saturable[10] or reverse saturable absorption[28] behaviors depending on the sample preparation method and the input laser fluence. Many new graphene-based hybrid materials have been prepared in the past few years[32-37], including PbS-decorated graphene nanosheets aiming at NIR photosensor applications[38-40], while their NLO performance has not been studied. Meanwhile, all the available synthetic methods for the graphene-PbS hybrid are generally complicated and do not produce uniform PbS QDs. It is noted that one important property of lead chalcogenide QDs is that they exhibit strong quantum confinement effect due to large exciton Bohr radius, so that their optical properties are very sensitive to particle size and shape. Therefore, a facile method for synthesizing high quality of graphene-PbS nanohybrid with well-controlled PbS particle shape and size distribution is urgently needed for the study of their NLO properties in NIR region.

The main motivation of this work is to extend the optical limiting performance of functionalized graphene from visible range to NIR by attaching uniform PbS QDs. Unlike previously reported tedious synthetic method, herein we have developed a facile route to prepare high-quality nanohybrid consisting of reduced graphene oxide (rGO) and PbS QDs (referred to as rGO-PbS). The third-order nonlinear absorption of the rGO-PbS nanohybrid were studied using open aperture Z-scan technique with a nanosecond pulsed laser at 532 nm and 1064 nm excitation. The as-prepared nanohybrid exhibited superior optical limiting properties compared to the individual component owning to significantly enhanced free carrier absorption.

Experimental Section

Synthesis of GO

GO was prepared from natural graphite powder by using a modified Hummers and Offeman's method with H_2SO_4 and $KMnO_4$ as oxidants [41, 42]. The as-prepared GO was suspended in ultrapure water to give a brown dispersion, which was subjected to a dialysis for 7 days to completely remove residual salts and acids. The resulting purified GO powders were dried under vacuum.

Synthesis of rGO-PbS nanohybrid

OLA capped rGO-PbS nanohybrid suspensions were prepared using a facile single-medium method. In a typical reaction, GO (5 mg), $PbCl_2$ (1 mmol, 0.28 g) was added to 5 mL of OLA at room temperature in sealed reaction system by ultrasonication at 200 W power for 4 hours, and the mixture was heated to about 160 °C under vacuum for 1 h to distill off volatiles. During the reaction, the $PbCl_2$-GO-OLA mixture turned into a homogeneous solution. Ar gas was subsequently admitted, and the mixture was left for 30 min under vigorous stirring. Sulfur powder (0.5 mmol, 32 mg) was dissolved in 2.5 mL of OLA by heating at 60 °C in oil bath to give a red-yellow S solution, which was thereafter injected into the $PbCl_2$-GO-OLA mixture at the same temperature. The reaction was monitored by measuring the near- and mid-IR absorption spectra. When the right absorption band edge was reached, the heating was stopped and the solution was cooled quickly, resulting into a black colloidal solution. The obtained solution was centrifuged for 3 min at 5,000 rpm to precipitate the excess $PbCl_2$ precursor. A minimum amount of ethanol was added to the supernatant to induce precipitation of the nanohybrid and the solutions were subsequently centrifuged. The resulted supernatant was discarded, and the precipitate was redispersed in chloroform. The eventual nanohybrid dispersions were dried under Ar gas stream and redispersed in chloroform to remove any trace of ethanol from the solution.

Preparation of rGO-PbS/PMMA thin film

Initially, rGO-PbS nanohybrid were dissolved in chloroform with a linear transmittance of 60% at 532 nm at room temperature. Thereafter, 0.3g PMMA was added to 5.0 ml of this solution under vigorous stirring for 6 hours. The mixed solution was then drop-cast on fused silica, baked for 1 hour at 50 ºC.

Characterization

TEM images were obtained using a FEI Tecnai G^2 F30 Twin microscope with a LaB6 filament operated at 300 kV. The samples were prepared by drop-casting the suspension onto holey carbon grids. XRD was performed on a PANalytical X′pert PRO using Bragg–Brentano geometry. The samples were prepared by drop-casting concentrated solutions onto silicon substrates. XRD patterns are compared to those of PbS (JCPDS #01078-1054). The collection of near- and mid-IR absorption spectra was performed on a Lambda 950 UV/VIS/NIR Spectrophotometer (Perkin Elmer). Raman spectra were measured with a Renishaw InVia Raman microscope at room temperature with a 633 nm line laser as the excitation source. The Z-scan technique was employed to measure the nonlinear optical properties of samples. Briefly, 4 ns (FWHM), 532 nm and 1064 nm laser pulses with a repetition rate of 10 Hz from a Q-switched Nd:YAG laser (Continuum, Model Surelite SL-I-10) was used as the light source. The spatial and temporal profiles of the laser pulses presented an approximately Gaussian distribution. The laser beam waist was 20 μm for the excitation wavelengths. Rayleigh lengths, Z_R, were 2.36 mm and 1.18 mm for the 532 nm and 1064 nm wavelength, respectively. The laser beam was split into two parts by a beam splitter and two corresponding pyroelectric detectors (Laser Probe, RJ-735; with RJ7620 dual channel power meter) were used to measure changes in laser transmission. Under the open-aperture configuration, the aperture placed before the detector was kept open and the nonlinear absorption of the samples was measured. The samples were placed in quartz cells with thickness of 2 mm, mounted on a translation stage that was controlled by a computer to move along the Z axis with respect to the focal point.

Results and Discussion

Inspired by our previous methods for the synthesis of PbSe and PbS_xSe_{1-x} QDs[10, 30] , we have developed a facile low-cost method to prepare rGO-PbS nanohybrid. Instead of employing the widely used but toxic trioctylphosphine (TOPO) as surfactant, we performed the entire synthesis in the more environment-friendly solvent of oleylamine (OLA), in which topologically controlled rGO-PbS nanohybrid could be obtained by a hot injection method. The synthesis procedure of the rGO-PbS nanohybrid is depicted in Figure 1. In a typical reaction, GO prepared via a modified Hummer's method[41, 42] and $PbCl_2$ were added to OLA at room temperature in a sealed flask, and treated by ultrasonication for 4 hours. In this process, Pb^{2+} can be attached onto the GO surface through coordination with various polar groups, like carboxylic acid groups. The hot S_8/OLA solution was then injected into the reaction mixture at 160 ℃. Under such conditions, the elemental sulfur reacts with Pb^{2+} to give PbS QDs while GO was also transformed into rGO[43, 44]. The color change of the reaction mixture from brown to dark black indicated the formation of rGO-PbS nanohybrid.

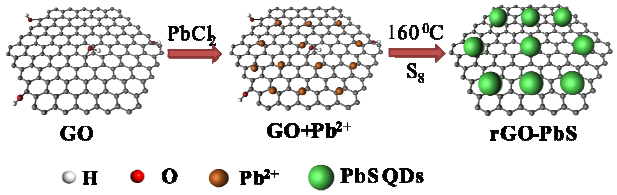

Figure 1. Schematic illustration of the synthesis procedure of rGO-PbS nanohybrid

For comparison purpose, we have also prepared PbS QDs under the same reaction conditions but in the absence of GO[45]. Figure 2a is a representative Transmission Electron Microscopy (TEM) image of the obtained PbS QDs, which shows monodispersed QDs with an average diameter of 8.5 nm±0.5 nm. The TEM image of the GO nanosheets (Figure 2b) used for synthesizing the nanohybrid shows that the GO mostly exist as large thin sheets with a width of several microns, and only slight corrugations are observed between the neighboring sheets. Note the quality of the graphene oxide plays an important role on producing high quality rGO-PbS nanohybrid, as we found that large and flat rGO surface are beneficial for anchoring PbS nanocrystals. Figure 2c indicates that the produced rGO-PbS nanohybrid contains highly regular spherical PbS QDs attached on the rGO sheets. The graphene sheets remain flat and the PbS QDs are densely assembled on its surface, where the PbS QDs exhibit a monodispersed size of 8.0±0.5 nm. We conducted statistical analysis on the PbS QDs in the absence/presence of graphene template, and the size distribution diagrams of the PbS QDs are provided in Supplemental Information (Figure S1). Clearly, in both cases, the PbS QDs exhibit very uniform size distribution with similar particle

diameters around ~8 nm. It is believed that graphene works not only as a substrate for PbS QDs binding, but also behaves as a surfactant to regulate the growth of PbS QDs[22] and hence resulting in uniform PbS QDs. Figure 2c also shows that there are areas on the graphene not been covered by the PbS QDs. The attachment of the PbS QDs on the surface of rGO is presumed to be mainly from coordination interaction between the PbS nanocrystals and the carboxyl groups on the latter, as evidenced by the following FTIR spectroscopic analysis. However, it was unavoidable that some PbS ODs were physically adsorbed on the rGO surface during the synthesis. As the final products were repeatedly washed for several times, some of the PbS ODs would be washed off and result in partially uncovered areas on the rGO surface. The high-resolution TEM (HRTEM) measurement (Figure 2d) indicates that the PbS QDs attached on the graphene surface exhibit high crystallinity, with clear lattice fringes free of stacking fault. The most obvious lattice fringes of the spherical PbS QDs have the lattice plane space of 2.98 Å, corresponding to the (200) planes. Meanwhile, the HRTEM images disclosed the geometrical dimensions, and in particular the lateral dimensions of the graphene-PbS hybrid sheets (Figure S2), which demonstrated uniform PbS QDs spread on the thin rGO sheets evenly. In addition, we also performed Atomic Force Microscopy (AFM) measurement and representative AFM height image of rGO-PbS nanohybrid is shown in Figure S3. AFM data indicates that the height of the PbS QDs is around 7 nm, while the typical thickness of rGO is 2-3 nm, implying 3-4 layers[41].

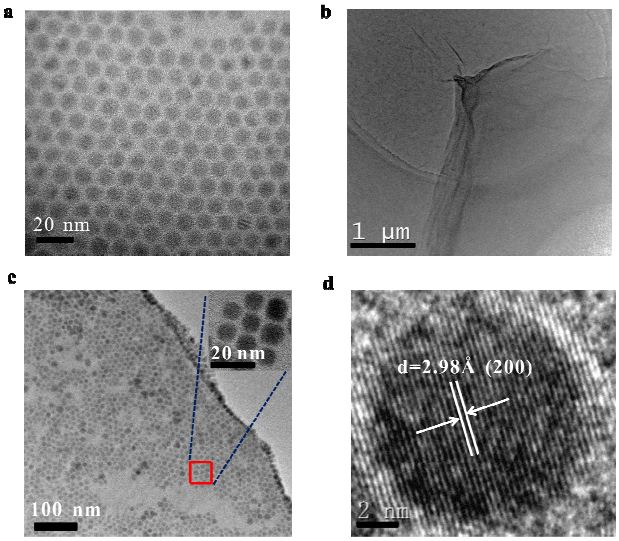

Figure 2. TEM images of (**a**) pure PbS QDs, (**b**) GO nanosheets, (**c**) rGO-PbS nanohybrid and (**d**) HRTEM image of PbS QDs grown on graphene .

The Fourier transform infrared (FTIR) and Raman spectra (Figure 3a and 3b) provide more information about the formation of the rGO-PbS nanohybrid. In the FTIR spectra, the peaks at 3401 (ν_{O-H}), 1733 ($\nu_{C=O}$), and 1629 cm^{-1} ($\nu_{C=C}$) are the characteristic peaks of the carboxyl and hydroxyl groups generated during the GO preparation[44, 46]. For the PbS QDs, the peaks at 2920, 2855 and 1458 cm^{-1}, can be assigned to the stretching of the C-H and N-H moieties of OLA. The disappearance of 3401(ν_{O-H}) at rGO-PbS samples implies the conversion of GO into chemically modified graphene sheets[43, 44]. The weakened peak at 1733 cm^{-1} ($\nu_{C=O}$) suggests the coordination interaction between the PbS nanocrystals and the carboxyl groups on GO[22]. In addition, the absence of the 1629 cm^{-1} peak indicates that coordination interaction influences the aromatic system in rGO. The Raman spectra (Figure 3b) of GO show four characteristic bands, including D band at 1336 cm^{-1}, G band at 1603 cm^{-1}, 2D band at 2637 cm^{-1} and D+G band at 2917 cm^{-1} that are consistent with literature reports[44]. As shown in Figure 3b, the characteristic band of PbS QDs is at 2882 cm^{-1} attributed to the surfactant of OLA. The rGO-PbS nanohybrid shows four bands with position similar to that of GO, suggesting that the Raman signals are mainly from the graphene component. However, the I_D/I_G ratio (1.03) of rGO-PbS nanohybrid is higher than that of GO (0.97), which is attributed to the presence of more defects due to interaction between the PbS QDs and the graphene sheets[44, 47]. The D+G band of rGO-PbS has higher intensity than that of GO due to the contribution from the OLA attached on the PbS QDs.

To further confirm the structure of the rGO-PbS produced by our method, the samples were subjected to the wide-angle powder X-ray diffraction (XRD) and the results are presented in the Figure 3c. The XRD pattern of GO shows a single peak at around 10.2°corresponding to the (002) plane, in agreement with literature value[46]. The three peaks at 25.8°, 29.9°, 42.9° corresponding to (111), (200), (220) planes for the PbS QDs are consistent with that of the standard PbS crystal structure (JCPDS #01078-1054)[38]. The rGO-PbS nanohybrid shows three XRD peaks at the same positions of PbS QDs, confirming that the PbS QDs have been successfully produced on graphene surface. No additional XRD peaks besides the PbS patterns were found for the rGO-PbS nanohybrid, ruling out the possibility of any other crystalline impurity. In addition, the rGO-PbS hybrid shows no XRD peaks at around 10.2°, indicating the conversion of GO into chemically modified graphene[46].

It is well known that when the sizes of semiconductor QDs are smaller than the bulk exciton Bohr radius, quantum confinement effect will occur[48]. As the particle size of our PbS QDs is much smaller than the Bohr radius (46 nm), strong quantum confinement leads to the shift of the absorption peak to 1487 nm, giving a well-resolved lowest-energy exciton transition in the NIR region. The rGO-PbS nanohybrid also exhibits a strong absorption at 1485 nm, indicating that the PbS QDs attached onto the graphene surface have nearly identical morphology as that of the pure PbS QDs. Keeping in mind that pristine graphene is highly transparent in the NIR region, Figure 3d indicates that the rGO-PbS dramatically improved the NIR absorption properties of the modified graphene.

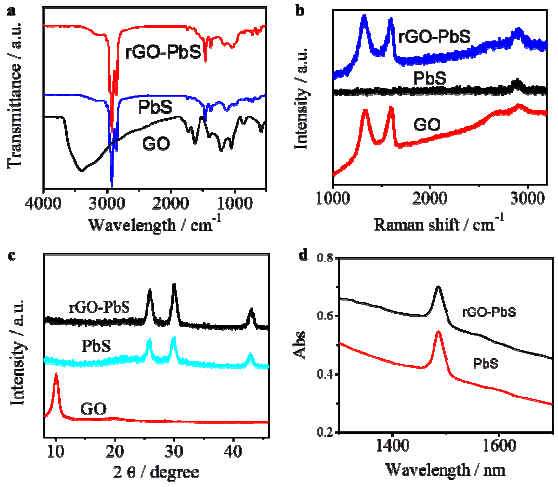

Figure 3. (**a**) Fourier transform infrared (FTIR) spectra, (**b**) Raman spectra, (**c**) XRD patterns and (**d**) NIR absorption spectra of the samples.

The optical limiting effects of the rGO-PbS nanohybrid were investigated by using the Z-scan technique. This technique can measure the optical nonlinearities by detecting the normalized sample transmittance of a Gaussian beam as a function of sample position (Z)[49]. Under the open-aperture condition, the normalized transmittance is measured as the sample translates through the focal plane of the focused beam. A normalized transmittance of 1 indicates that the material exhibits no NLO behavior. In the case of reverse saturable absorption, the transmittance would decrease with the power increase. A normalized transmittance above 1 otherwise indicates that the sample exhibits saturable absorption.

Figure 4 represents the open-aperture Z-scan curves of the GO, PbS QDs, rGO-PbS nanohybrid and C_{60} at various incident energies. C_{60} is a well-studied nonlinear optical material and frequently used as a reference for optical limiting in the visible range. The linear transmittances of all the samples were adjusted to be T = 55% at 532 nm and 70% at 1064 nm. The input laser pulse energy was 25 μJ at 532 nm and 100 μJ at 1064 nm, respectively. Clearly, from Figure 4, all of the curves have only valley at the focus. The deepest valley implies the best optical limiting performance. As shown in Figure 4a, rGO-PbS nanohybrid and C_{60} display significantly stronger optical limiting effects at 532 nm than GO and PbS QDs. Under the 1064 nm excitation (Figure 4c), the optical limiting properties of rGO-PbS are also much better than GO and PbS QDs, while C_{60} even showed no nonlinear absorption properties at this wavelength.

For more quantitative analysis, we fitted the Z-scan curves using the following equation[19, 51]:

$$\alpha = \frac{\alpha_0}{1 + I/I_s} + \beta I \qquad \text{(equation 1)}$$

where α_0, I and β are the linear absorption coefficients, incident laser intensity, and nonlinear absorption coefficient, respectively. β is concentration-dependent, corresponding to RSA or TPA at high intensity regime. I_s is the saturation intensity, which corresponds to the SA response occurring at low intensity regime and is concentration-independent. Using the following equation 2, the laser intensity as a function of the propagation depth in the thin sample z' is calculated:

$$\frac{dI}{dz'} = -\alpha(I) \cdot I \qquad \text{(equation 2)}$$

Eventually at each z position, the transmittance was computed through intensity distribution integration method. The measured Z-scan data are thus fitted to give the parameters of I_s and β. In Figure 4, the solid curves represent numerical data fitting. It shows that β, the nonlinear absorption coefficient (7.9×10^{-10} m / W) for rGO-PbS is eight times larger than that of GO (1.0×10^{-10} m / W), and is also higher than that of the C_{60} reference (6.8×10^{-10} m / W). The valley-shaped curves of rGO-PbS indicate pure optical limiting behavior. Figure 4b and 4d show the normalized transmittance versus input fluence characteristic and theoretically fitted curves. With 532 nm laser, the optical limiting thresholds *Ft* (input fluence at which the transmission drops to 50% of the linear transmission) of the rGO-PbS is found to be 2.3 J / cm^2, which is significantly lower than that of GO and PbS QDs, very similar to that of C_{60} (Figure 4b). Under 1064 nm excitation, the *Ft* of the rGO-PbS is found to be 10 J / cm^2, which is also much lower than that of GO and PbS QDs (Figure 4d). It is worth noting that the low *Ft* value of the rGO-PbS at 1064 nm suggests useful applications in fabricating high performance optical products in the NIR region. The results indicate the attached PbS QDs on the graphene surface give rise to significantly improved optical limiting properties compared with the individual GO and PbS QDs. As β values can vary dramatically with sample concentration, we also performed Z-scan measurements for rGO-PbS nanohybrid at different concentrations, as shown in Figure 4e and f. With increased sample concentration, corresponding linear transmittance varied from 0.81 to 0.29, the β values became almost 5 times larger, *i.e.*, varied from 2.5×10^{-10} m/W to 1.2×10^{-9} m/W.

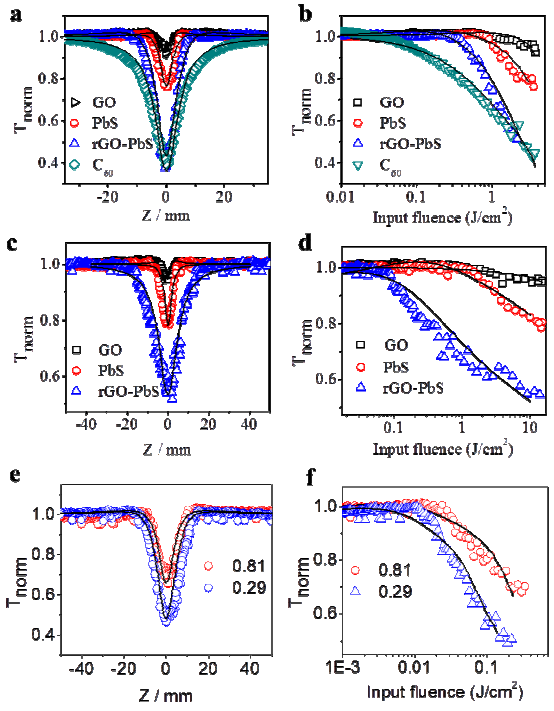

Figure 4. Open aperture Z-scan data (symbols) and theoretically fitted curves (solid curves) using (**a**) 4 ns pulses at 532 nm and (**c**) 4 ns pulses at 1064 nm. Plot of transmittance versus input fluence and theoretically fitted curves (solid curves) using (**b**) 4 ns pulses at 532 nm and (**d**) 4 ns pulses at 1064 nm. The solution spectra were collected in a 2.0 mm path length cell. The linear transmittance of all the above samples given by the F_{out}/F_{in} ratio in the limit of zero fluence is 0.55 at 532 nm and 0.7 at 1064 nm. T_{norm} is the measured transmittance normalized by the linear transmittance of the sample. (**e**) Open Z-scan data (symbols) and theoretically fitted curves (solid curves) using 4 ns pulses at 532 nm for rGO-PbS nanohybrid at different concentrations (linear transmittance 0.81 or 0.29), (**f**) corresponding plot of transmittance versus input fluence and theoretically fitted curves (solid curves)

The third-order nonlinear absorption of nanomaterials can be affected by many factors. In most cases, the mechanism is dependent on both the intrinsic properties of nanomaterials and the incident laser pulse[1]. In solution, when the nanomaterials have high absorption cross section and small radius of curvature, the solvent evaporates and micro bubble will form around the nanomaterials due to laser-induced heating. These micro bubbles then cause thermal induced nonlinear scattering, which has been found in the case of carbon nanotubes[14], graphene[2] and their composites with an appearance of reverse saturable absorption[13, 44]. The lifetimes of the micro bubbles were reported to be around several nanoseconds[52]. It should be noted that materials that exhibit optical limiting performance arising from such micro bubble effect are unlikely to be

applied in solid devices. Another important mechanism could contribute to the optical limiting properties is free carrier absorption, which is usually found in semiconductors[1, 5, 53]. In this process, the electrons can be promoted to higher states in the conduction band by absorbing additional photons, which is similar to the excited-state absorption in a molecular system. The intensity of the free carrier absorption is dependent on the carrier population as the laser energy is absorbed[1].

In our study, the mechanism of the optical limiting properties of rGO-PbS system is expected to be a result of combination of free carrier absorption and nonlinear scattering[30, 44]. According to the above results, the rGO-PbS show much better optical limiting properties than its individual compartments, *i.e.*, rGO and PbS QDs, suggesting the occurrence of synergetic effects. We believe this superior optical limiting performance of rGO-PbS arises from the following effects. Because of the coordination interaction between PbS QDs and rGO substrate, strong coupling between these two components can take place. When the PbS QDs absorb the laser energy, it could transfer the electron and energy to the rGO (Figure 5) [22, 40], which could enhance the free-carrier cross section[1, 22, 44]. Hence the rGO-PbS show better optical limiting properties induced by an enhancement of free carrier absorption. Meanwhile, the energy is efficiently transferred into solution from the large surface area of rGO. Then thermal energy generates a large quantity of bubbles which may cause strong nonlinear scattering effect also responsible for the drastic enhancement of optical limiting performance[22, 54]. Previous angular dependence scattering measurement has confirmed such effect[19, 53], indicating the nonlinear scattering effect contributed to the optical limiting effects of PbS nanoparticles[53], graphene and graphene-based materials[55, 56].

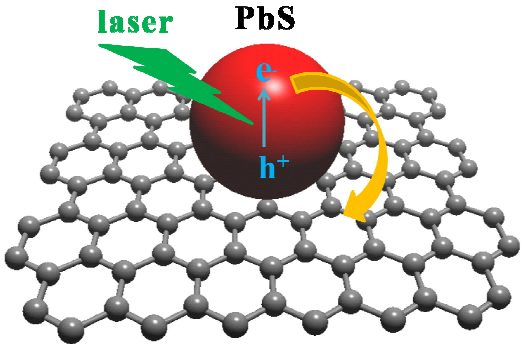

Figure 5. Schematic illustration of charge and energy transfer between PbS QDs and rGO

It is known that the optical limiting performance stemming from the bubble effect can only occur in solution, while the free carrier absorption should exist in both solution and solid state. To further understand the contribution of these two effects, we studied the third-order nonlinear absorption effect of the rGO-PbS nanohybrid in solid state. The rGO-PbS nanohybrid can be conveniently prepared into poly(methyl methacrylate) (PMMA) thin films by mixing them in chloroform solution and then spin cast onto glass substrate. From the inset of Figure 6, it can be seen that the nanohybrid have been homogeneously incorporated into solid-state PMMA and the glass slide coated with thin film shows a high transparency. The rGO-PbS nanohybrid films showed good optical limiting properties when the input laser pulse was 13.4 μJ at 532 nm laser and 193 μJ at 1064 nm (Figure 6). In addition, the optical limiting effect becomes even stronger with increasing input laser power (Figure S4). Since nonlinear scattering resulted from the bubbles forming can be ruled out in the thin films, it is reasonable to attribute free carrier absorption process as the dominant contribution to the NLO performance of the solid-state rGO-PbS nanohybrid. This result suggests that the rGO-PbS nanohybrid thin films have great potential as excellent NLO material for optical limiting applications in both visible and NIR region.

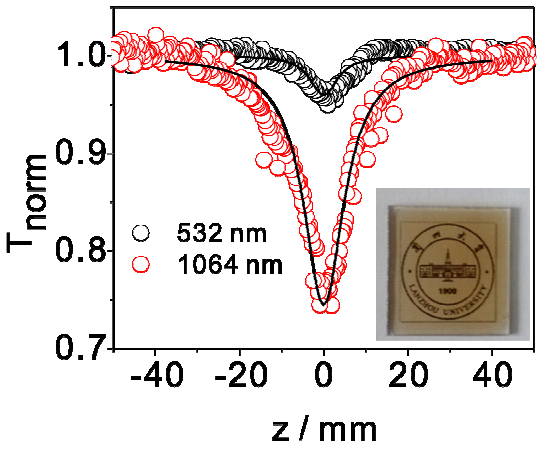

Figure 6. Open aperture Z-scan data (symbols) and theoretically fitted curves (solid curves) for a neat film of rGO-PbS in poly(methyl methacrylate) irradiated by 4 ns pulses at 532 nm and 1064 nm. The linear transmittance of the sample given by the F_{out}/F_{in} ratio in the limit of zero fluence is 0.65 at 532 nm and 0.85 at 1064 nm. Inset: photograph of film cast on fused silica.

Conclusions

In summary, we have developed a facile, low-cost, and phosphine-free method to synthesize novel rGO-PbS nanohybrid consisting of uniform PbS QDs assembled on the rGO surface. Then we thoroughly studied the nonlinear optical properties of the hybrid and find that the rGO-PbS nanohybrid shows giant broadband optical limiting response from visible region to NIR region surpass GO and PbS QDs. The mechanism of the optical limiting properties is believed to arise from an efficient charge and energy transfer between the PbS QDs and rGO that enhances both the free carrier absorption and nonlinear scattering processes. Furthermore, the nanohybrid in polymer thin films also showed good optical limiting properties with high transparency. These results reveal that directly attaching uniform rGO-PbS particles onto chemically modified rGO can dramatically enhance the third-order nonlinear absorption of rGO in both visible and NIR region, which opens a new way in design developing broadband laser-protecting coating and optoelectronic devices.

Acknowledgements

The acknowledgements come at the end of an article after the conclusions and before the notes and references. This work is supported by National Basic Research Program of China (973 Program) No.2012CB933102, National Natural Science Foundation of China (NSFC. 21233001, 21190034，21073079, J1103307), Specialized Research Fund for the Doctoral Program of Higher Education (SRFDP. 20110211130001), the Fundamental Research Funds for the Central Universities and 111 Project.

Notes and references

[a] State Key Laboratory of Applied Organic Chemistry, College of Chemistry and Chemical Engineering, Key Laboratory of Special Function Materials and Structure Design (MOE), Lanzhou University, Lanzhou 730000, P. R. China.
E-mail: haoli.zhang@lzu.edu.cn; qiangwang@lzu.edu.cn;
[b] School of Physical Science and Technology, Soochow University, Suzhou 215006, P. R. China
[c] Department of Physics, Harbin Institute of Technology, Harbin 150001, P. R. China
E-mail: ylsong@hit.edu.cn

1. L. W. Tutt and T. F. Boggess, *Progress in Quantum Electronics*, 1993, **17**, 299-338.
2. M. Feng, H. B. Zhan and Y. Chen, *Appl. Phys. Lett.*, 2010, **96**, 033107.
3. G. K. Lim, Z. L. Chen, J. Clark, R. G. S. Goh, W. H. Ng, H. W. Tan, R. H. Friend, P. K. H. Ho and L. L. Chua, *Nat. Photonics*, 2011, **5**, 554.
4. G. J. Zhou and W. Y. Wong, *Chem. Soc. Rev.*, 2011, **40**, 2541.
5. R. Philip, P. Chantharasupawong, H. Qian, R. Jin and J. Thomas, *Nano Lett.*, 2012, **12**, 4661.
6. S. V. Rao, D. N. Rao, J. A. Akkara, B. S. DeCristofano and D. V. G. L. N. Rao, *Chem. Phys. Lett.*, 1998, **297**, 491.
7. H. Lei, H. Z. Wang, Z. C. Wei, X. J. Tang, L. Z. Wu, C. H. Tung and G. Y. Zhou, *Chem. Phys. Lett.*, 2001, **333**, 387.
8. J. Balapanuru, J. X. Yang, S. Xiao, Q. Bao, M. Jahan, L. Polavarapu, J. Wei, Q. H. Xu and K. P. Loh, *Angew. Chem. Int. Ed.*, 2010, **49**, 6549.
9. L. Wang, Y. Zhao, J. Guan and F. Wu, *Appl. Phys. Lett.*, 2013, **102**, 251906.
10. D. J. Asunskis, I. L. Bolotin and L. Hanley, *J. Phys. Chem. C*, 2008, **112**, 9555.
11. T. M. Wang, B. Gao, Q. Wang, M. Zhao, K. B. Kang, Z. G. Xu and H. L. Zhang, *Chem. Asian J.*, 2013, **8**, 912.
12. Y. Zeng, C. S. Wang, F. L. Zhao, M. Qin, Y. Zhou and X. B. Huang, *Appl. Phys. Lett.*, 2013, **102**, 043308.
13. H. X. Wu, D. D. Liu, H. Q. Zhang, C. Y. Wei, B. Zeng, J. L. Shi and S. P. Yang, *Carbon*, 2012, **50**, 4847.
14. B. Anand, R. Podila, P. Ayala, L. Oliveira, R. Philip, S. S. Sai, A. A. Zakhidov and A. M. Rao, *Nanoscale*, 2013, **5**, 7271.
15. Z. B. Liu, Y. Wang, X. L. Zhang, Y. F. Xu, Y. S. Chen and J. G. Tian, *Appl. Phys. Lett.*, 2009, **94**, 021902.
16. Z. B. Liu, X. L. Zhang, X. Q. Yan, Y. S. Chen and J. G. Tian, *Chinese Science Bulletin*, 2012, **57**, 2971.
17. S. Husaini, J. E. Slagle, J. M. Murray, S. Guha, L. P. Gonzalez and R. G. Bedford, *Appl. Phys. Lett.*, 2013, **102**, 191112.
18. Y. Liu, J. Zhou, X. Zhang, Z. Liu, X. Wan, J. Tian, T. Wang and Y. Chen, *Carbon*, 2009, **47**, 3113.
19. N. Liaros, P. Aloukos, A. Kolokithas-Ntoukas, A. Bakandritsos, T. Szabo, R. Zboril and S. Couris, *J. Phys. Chem. C*, 2013, **117**, 6842.
20. W. Song, C. He, W. Zhang, Y. Gao, Y. Yang, Y. Wu, Z. Chen, X. Li and Y. Dong, *Carbon*, 2014, **77**, 1020.
21. H.-X. Wang, Q. Wang, K.-G. Zhou and H.-L. Zhang, *Small*, 2013, **9**, 1266.
22. W. Wei, T. He, X. Teng, S. Wu, L. Ma, H. Zhang, J. Ma, Y. Yang, H. Chen, Y. Han, H. Sun and L. Huang, *Small*, 2012, **8**, 2271.
23. Y. F. Xu, Z. B. Liu, X. L. Zhang, Y. Wang, J. G. Tian, Y. Huang, Y. F. Ma, X. Y. Zhang and Y. S. Chen, *Adv. Mater.*, 2009, **21**, 1275.
24. Y. Zhou, Q. Bao, L. A. L. Tang, Y. Zhong and K. P. Loh, *Chem. Mater.*, 2009, **21**, 2950.
25. N. Liaros, E. Koudoumas and S. Couris, *Appl. Phys. Lett.*, 2014, **104**, 191112.
26. V. Besse, A. Fortin, G. Boudebs, P. S. Valle, M. Nalin and C. B. de Araujo, *Appl. Phys. B-Lasers and Optics*, 2014, **117**, 891.
27. Q. Bellier, N. S. Makarov, P. A. Bouit, S. Rigaut, K. Kamada, P. Feneyrou, G. Berginc, O. Maury, J. W. Perry and C. Andraud, *Phys. Chem. Chem. Phys.*, 2012, **14**, 15299.
28. H. S. Kim and K. B. Yoon, *J. Am. Chem. Soc.*, 2012, **134**, 2539.
29. S. A. McDonald, G. Konstantatos, S. Zhang, P. W. Cyr, E. J. Klem, L. Levina and E. H. Sargent, *Nat. Mater.*, 2005, **4**, 138.
30. M. S. Neo, N. Venkatram, G. S. Li, W. S. Chin and J. Wei, *J. Phys. Chem. C*, 2009, **113**, 19055.
31. C. Li, G. Shi, H. Y. Xu, S. Y. Guang, R. H. Yin and Y. L. Song, *Mater. Lett.*, 2007, **61**, 1809.
32. C. Tan, X. Huang and H. Zhang, *Mater. Today*, 2013, **16**, 29.
33. X. Cao, Z. Zeng, W. Shi, P. Yep, Q. Yan and H. Zhang, *Small*, 2013, **9**, 1703.
34. X. Cao, B. Zheng, X. Rui, W. Shi, Q. Yan and H. Zhang, *Angew. Chem. Int. Ed.*, 2014, **53**, 1404.
35. X. Huang, S. Li, Y. Huang, S. Wu, X. Zhou, S. Li, C. L. Gan, F. Boey, C. A. Mirkin and H. Zhang, *Nat. Commun.*, 2011, **2**, 292.
36. X. Huang, X. Zhou, S. Wu, Y. Wei, X. Qi, J. Zhang, F. Boey and H. Zhang, *Small*, 2010, **6**, 513.
37. S. Wu, Q. He, C. Zhou, X. Qi, X. Huang, Z. Yin, Y. Yang and H. Zhang, *Nanoscale*, 2012, **4**, 2478.
38. S. Ghosh, T. Pal, D. Joung and S. I. Khondaker, *Appl. Phys. A*, 2012, **107**, 995.
39. Z. Sun, Z. Liu, J. Li, G. A. Tai, S. P. Lau and F. Yan, *Adv. Mater.*, 2012, **24**, 5878.
40. D. Zhang, L. Gan, Y. Cao, Q. Wang, L. Qi and X. Guo, *Adv. Mater.*, 2012, **24**, 2715.
41. N. N. Chai, J. Zeng, K. G. Zhou, Y. L. Xie, H. X. Wang, H. L. Zhang, C. Xu, J. X. Zhu and Q. Y. Yan, *Chem. Eur. J.*, 2013, **19**, 5948.
42. W. S. Hummers and R. E. Offeman, *J. Am. Chem. Soc.* , 1958, **80**, 1339.
43. H. Wang, J. T. Robinson, X. Li and H. Dai, *J. Am. Chem. Soc.*, 2009, **131**, 9910.
44. M. K. Kavitha, H. John, P. Gopinath and R. Philip, *J. Am. Chem. Soc*, 2013, **1**, 3669.
45. B. Gao, M. Zhao, Q. Wang, K.-B. Kang, Z.-G. Xu and H.-L. Zhang, *New J. Chem.*, 2013, **37**, 1692.
46. X. Y. Yu, Z. H. Chen, D. B. Kuang and C. Y. Su, *ChemPhysChem*, 2012, **13**, 2654.
47. Q.-P. Luo, X.-Y. Yu, B.-X. Lei, H.-Y. Chen, D.-B. Kuang and C.-Y. Su, *J. Phys. Chem, C*, 2012, **116**, 8111.
48. C. B. Murray, S. H. Sun, W. Gaschler, H. Doyle, T. A. Betley and C. R. Kagan, *IBM Journal of Research and Development*, 2001, **45**, 47-56.
49. M. Sheikbahae, A. A. Said, T. H. Wei, D. J. Hagan and E. W. Vanstryland, *IEEE Journal of Quantum Electronics*, 1990, **26**, 760.
50. Z. B. Liu, Y. F. Xu, X. Y. Zhang, X. L. Zhang, Y. S. Chen and J. G. Tian, *J. Phys. Chem. B*, 2009, **113**, 9681.
51. K. G. Zhou, M. Zhao, M. J. Chang, Q. Wang, X. Z. Wu, Y. Song and H. L. Zhang, *Small*, 2015, **11**,694
52. V. Kotaidis, C. Dahmen, G. von Plessen, F. Springer and A. Plech, *J. Chem. Phys.*, 2006, **124**,184702.

53. Q. S. Li, C. L. Liu, L. Y. Zang, Q. H. Gong, X. L. Yu and C. B. Cao, *Laser Phys.*, 2008, **18**, 434.
54. A. Midya, V. Mamidala, J.-X. Yang, P. K. L. Ang, Z.-K. Chen, W. Ji and K. P. Loh, *Small*, 2010, **6**, 2292.
55. J. Wang, Y. Hernandez, M. Lotya, J. N. Coleman and W. J. Blau, *Adv. Mater.*, 2009, **21**, 2430.
56. Y. Gan, M. Feng and H. Zhan, *Appl. Phys. Lett.*, 2014, **104**, 171105.

TOC: "**Broadband Optical Limiting Response of Graphene-PbS Nanohybrid**"

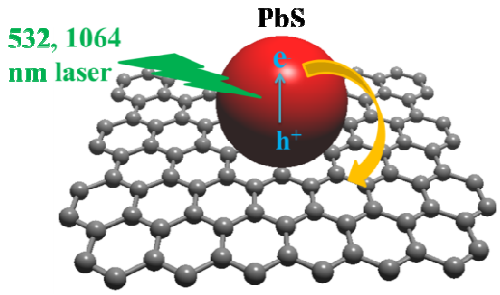

We have developed a facile method to synthesize novel rGO-PbS nanohybrid which exhibited excellent optical limiting properties upon both 532 nm and 1064 nm irradiations.